Nonclassicality and Phase Estimation of Hybrid Squeezed States

Mohammad Bohloul[1], Jia-Xin Peng[2], Mohamed Amazioug[3], P. Najmadi[4], and S.K. Singh[5*]

[1]Department of Theoretical Physics and Astrophysics, University of Tabriz, Tabriz 51666, Iran

[2]School of Physical Science and Technology, Nantong University, Nantong 226019, China

[3]LPTHE-Department of Physics, Faculty of Sciences, Ibnou Zohr University, Agadir, Morocco

[4]Department of Mathematics, Payame Noor University,P.O.Box 19395-3697,Tehran,Iran.

[5]Department of Physics, Akal University, Talwandi Sabo, Bathinda 151302, India

September 1, 2026

Abstract

We present a theoretical study on the generation and nonclassical properties of hybrid squeezed states (HSS), a class of engineered quantum states with enhanced quantum features. Using a modified beam splitter-Kerr medium scheme, we construct superpositions of squeezed vacuum and two-photon-added squeezed states, providing a flexible framework to generate and control hybrid quantum states. Nonclassicality is analysed via Mandel's Q parameter, photon number distributions, probability distribution functions, and Wigner functions, revealing sub-Poissonian statistics, oscillatory photon distributions, and significant Wigner negativity. Phase-sensitivity analysis within a Mach-Zehnder interferometric framework demonstrates that HSS outperform conventional squeezed and photon-added squeezed states, achieving measurement precisions that exceed the standard quantum limit and approach the Heisenberg limit under optimal parameters. These results establish hybrid squeezed states as a powerful resource for quantum metrology, communication, and optical interferometry.

Keywords: Squeezed state, Wigner function, Mandel Parameter, Degenerate parametric amplifier, Nonclassicality

1. Introduction

In quantum information protocols, coherent and squeezed states are among the most important states of the electromagnetic field, with wide-ranging applications in various domains of modern era quantum technology. [1–9]. These states were first introduced in the second half of the twentieth century and have since been extensively studied. Coherent states, introduced by Roy J. Glauber [10], are considered the quantum states closest to classical waves. These states are produced in high-quality lasers and exhibit quasi-classical behavior [11]. Squeezed states were introduced in the 1980s as states with reduced uncertainty [12,13]. These states are particularly significant because they can reduce the uncertainty in one canonical variable (position

*Corresponding author. E-mail: singhshailendra3@gmail.com

or momentum) below the standard quantum limit, although this reduction comes at the expense of increased uncertainty in the conjugate variable. This unique characteristic makes squeezed states a valuable tool in quantum metrology [14]. In recent years, the generation and control of squeezed states have witnessed remarkable progress. Very recently, researchers have successfully generated squeezed vacuum sources with unprecedented stability and a squeezing level of 4.3 dB (equivalent to 5.9 dB without losses) in rubidium vapor using artificial intelligence control, which automatically adapts to environmental disturbances [21]. This achievement demonstrates the synergy between artificial intelligence and fundamental science in overcoming the complexity limitations of quantum systems. In other domains, the squeezing frequency band has been extended to the millihertz range, which is crucial for gravitational wave detectors [22]. Additionally, the generation of bright squeezed light in the kilohertz frequency band [23], and the proposal of a scheme for extracting and stably controlling 40 pairs of entangled sideband modes from a single squeezed state [24], represent significant steps toward high-capacity quantum communication networks. These advances make the applications of squeezed states in quantum metrology, secure communications, and fault-tolerant quantum computing more practical and tangible. The properties of coherent states include their special behavior with respect to the annihilation operator, Poissonian photon statistics, and minimum uncertainty [11]. In contrast, squeezed states exhibit non-Poissonian photon statistics and asymmetric uncertainty [12,13] From a theoretical perspective, coherent states are inherently classical, while squeezed states are fundamentally nonclassical. However, by applying photon addition or subtraction operators to coherent states, nonclassical states can be achieved [15]. Squeezed states can also exhibit rich nonclassical features through photon addition or subtraction, as reported in [16]. Squeezed number states can also exhibit nonclassical features, as shown in [17]. A scheme was proposed for generating photon-added coherent states without actual photon addition, resulting in states with remarkable nonclassical properties [20]. Furthermore, Photon-added states, which include photon-added coherent states (PACS) and photon-added squeezed states (PASS), are engineered states that exhibit pronounced nonclassical features. Nonclassical behavior of such states is typically measured through various criteria, such as negativity of the Wigner function, sub-Poissonian statistics, and quantum squeezing.

2. Hybrid state production

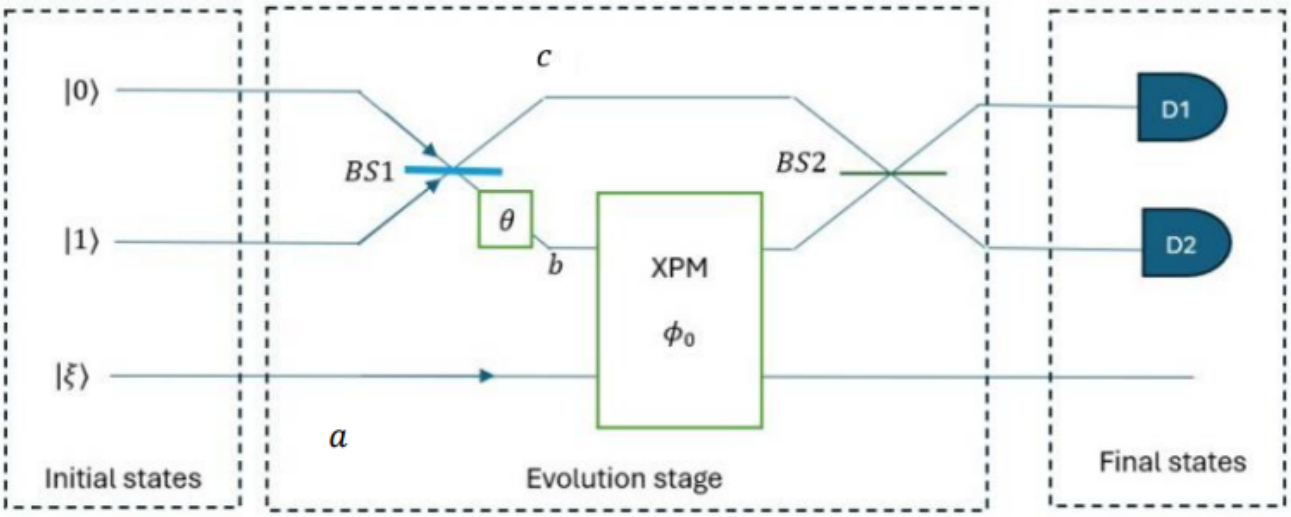


Figure 1: (Color online) Schematic diagram to produce Hybrid Squeezed States. Panels (a) and (c) have been corrected to properly indicate the input and output modes of the beam splitter and Kerr medium.

Here, by modifying the schematically shown scheme in [22], a new design is introduced. In this design, a single photon is first sent to a beam splitter (BS1) for Pre-selection. The output state is as follows:

$$|\psi_s\rangle = \frac{1}{\sqrt{2}}\left(|1\rangle_b|0\rangle_c + i|0\rangle_b|1\rangle_c\right) \tag{1}$$

The output of path b enters a Kerr environment after a phase shift of θ along with a squeezed state. The squeezed state $|\xi\rangle$ and the single photon interact through the Kerr medium. The Squeezed state as follows, [17]

$$|\xi\rangle = S(\xi)|0\rangle = (\cos|\xi|)^{-1/2}\sum_{k=0}^{\infty}\frac{\sqrt{(2k)!}}{2^k k!}\tanh(|\xi|)^k|2k\rangle, \xi = re^{i\theta}. \tag{2}$$

A squeezed state is parameterized by $0 \leq r$ (the squeezing magnitude) and $0 \leq \theta < 2\pi$ (the squeezing angle). And the Hamiltonian of the Kerr environment is as follows [22].

$$H_I = \hbar\chi a^\dagger a b^\dagger b = \hbar\chi\hat{n}_a\hat{n}_b \tag{3}$$

We can write the time evolution operator using this Hamiltonian as $U = Exp(-iH\tau/\hbar)$, and the evoluted state is obtained by applying this unitary operator as follows.

$$\begin{aligned} |\Psi'\rangle &= U|\xi\rangle_a \otimes |\psi_i'\rangle_{b,c} = \exp\left(-i\phi_0\hat{n}_a\hat{n}_b\right)|\xi\rangle_a \otimes |\psi_i'\rangle_{b,c} \\ &\approx \left(1 - i\phi_0\hat{n}_a \otimes \hat{n}_b\right)|\xi\rangle_a \otimes |\psi_i'\rangle_{b,c} \end{aligned} \tag{4}$$

And where $\phi_0 = \chi t$. We add a phase shifter in mode b so that the state $|\psi_i\rangle$ before interacting with the signal is changed to $|\psi_i'\rangle = \frac{1}{\sqrt{2}}(e^{i\theta}|1\rangle_b|0\rangle_c + i|0\rangle_b|1\rangle_c)$. So, the output state is as follows.

$$|\psi_i'\rangle = \frac{1}{\sqrt{2}}\left(e^{i\theta}|1\rangle_b|0\rangle_c + i|0\rangle_b|1\rangle_c\right) \tag{5}$$

$$|\Psi'\rangle = \frac{1}{\sqrt{2}}\left\{e^{i\theta}\left(|\xi\rangle_a|1\rangle_b - i\phi\hat{n}_a|\xi\rangle_a \otimes \hat{n}_b|1\rangle_b\right)|0\rangle_c + i\left(\left(|\xi\rangle_a|0\rangle_b - i\phi\hat{n}_a|\xi\rangle_a \otimes \hat{n}_b|0\rangle_b\right)|1\rangle_c\right)\right\} \tag{6}$$

$$= \frac{1}{\sqrt{2}}\left\{e^{i\theta}|\xi\rangle_a|1\rangle_b|0\rangle_c - ie^{i\theta}\phi\hat{n}_a|\xi\rangle_a \otimes \hat{n}_b|1\rangle_b|0\rangle_c + i|\xi\rangle_a|0\rangle_b|1\rangle_c + \phi\hat{n}_a|\xi\rangle_a \otimes \hat{n}_b|0\rangle_b|1\rangle_c\right\} \tag{7}$$

$$= \frac{1}{\sqrt{2}}\left\{e^{i\theta}|\xi\rangle_a|1\rangle_b|0\rangle_c + i|\xi\rangle_a|0\rangle_b|1\rangle_c - i\phi e^{i\theta}\hat{n}_a|\xi\rangle_a|1\rangle_b|0\rangle_c\right\} \tag{8}$$

Then, the output states of b and c interfere with each other in an unbalanced beam splitter BS2 with the transition $\mathbf{t}$ and the reflection coefficient $\mathbf{s}\left(t^2+s^2=1\right)$.. If detector D1 detects a photon, the output state is post-selected [22].

$$|\psi_r\rangle_{1d} = t|1\rangle_b|0\rangle_c + s|0\rangle_b|1\rangle_c \tag{9}$$

The final state in path of A, and the post-selected process in paths b and c is obtained as follows:

$$\begin{aligned} |\Phi\rangle_a &=_{b,c} \langle\psi_r|\Psi'\rangle_{a,b,c} \\ &= \frac{1}{\sqrt{2}}\left(e^{i\theta}t + is\right)|\xi\rangle_a - ie^{i\theta}\frac{t\phi_0}{\sqrt{2}}a^\dagger a|\xi\rangle_a. \end{aligned} \tag{10}$$

On the other hand, we know that [21]

$$\begin{aligned} a|\xi\rangle &= \xi\sqrt{M_1(|\xi|)}|\xi,1\rangle \\ \xi\sqrt{M_1(|\xi|)}a^\dagger|\xi,1\rangle &= \xi\sqrt{M_2(|\xi|)}|\xi,2\rangle \end{aligned} \tag{11}$$

Taking into account the above $\xi = r$ and $\theta = -\pi/2$, the final state is as follows.

$$\begin{aligned} |\phi\rangle &= \alpha|\xi\rangle + \beta|\xi,2\rangle \\ \alpha = i\frac{s-t}{\sqrt{2}}, &\quad \beta = -\frac{t\phi_0\xi\sqrt{M_2(|\xi|)}}{\sqrt{2}} \end{aligned} \tag{12}$$

Where $|\xi,2\rangle$ is two photon added squeezed state [17].

$$|\xi,2\rangle := \frac{\left(a^\dagger\right)^2}{\sqrt{M_2(|\xi|)}}|\xi\rangle = \frac{\left(1-|\xi|^2\right)^{\frac{1}{4}}}{\sqrt{M_2(|\xi|)}}\sum_{k=0}^{\infty}\left(\frac{\xi}{2}\right)^k\frac{\sqrt{(2k+2)!}}{k!}|2k+2\rangle \tag{13}$$

where the normalization factor $M_2(|\xi|)$ is derived in terms of the Legendre polynomials, i.e. $M_2(|\xi|) = 2!\left(1-|\xi|^2\right)^{-1}\mathrm{P}_2\left(\left(1-|\xi|^2\right)^{\frac{-1}{2}}\right)$. $|\Phi\rangle$ is a superposition state between the squeezed state and the two-photon added squeezed state. If the second beam splitter was balanced, $t = s = 1/\sqrt{2}$, the output state is the two-photon added squeeze state. And if $t \to 0$, the output state is a squeezed state. Next, we need to normalize the output state.

$$|\phi\rangle = \frac{1}{\mathrm{N}}(\alpha|\xi\rangle + \beta|\xi,2\rangle) \tag{14}$$

$$\mathrm{N} = 1/\sqrt{\alpha^2+\beta^2+\gamma^*\alpha\beta^* + \gamma\alpha^*\beta} \tag{15}$$

$$\gamma = \langle\xi \mid \xi,n\rangle = \frac{\left(1-|\xi|^2\right)^{\frac{1}{2}}\left(\frac{\xi}{2}\right)^{\frac{-n}{2}}}{\sqrt{M_n(|\xi|)}}\frac{1}{\left(\frac{-n}{2}\right)!}{}_2F_1\left(\frac{1}{2},1;\frac{-n}{2}+1;|\xi|^2\right) \tag{16}$$

With the help of relation $\frac{9.101}{1}$ from [18], one can easily show that when n is a positive even number, the expression γ is not equal to zero. Here, N is the normalization constant and γ is the superposition of the vacuum squeezed state and the two-photon-added squeezed state. For $n = 2$, this is as follows:

$$\gamma_{n=2} = \langle \xi \mid \xi, 2 \rangle = \frac{\left(1 - |\xi|^2\right)^{-3} \cdot |\xi|^9}{\sqrt{M_6(|\xi|)}}. \tag{17}$$

3. Results and Discussion

In the following, we will investigate the non-classical features of the state, which is it hybrid squeezed state ($|\phi\rangle$) by using Mendel's Q parameter, the photon number distribution function, and the Wigner function.

3.1. Q-parameter

In the following, we will investigate the non-classical features of the state $|\phi\rangle$ by using Mendel's Q parameter, which is defined as follows [27,28,41].

$$Q = \frac{\langle n^2 \rangle}{\langle n \rangle} - \langle n \rangle - 1 \tag{18}$$

The statistical properties of the output state can be characterized as follows: $Q = 0$ corresponding to Poissonian photon statistics,

$Q > 0$ corresponding to, super-Poissonian photon statistics and

$Q < 0$ corresponding to, sub-Poissonian photon statistics.

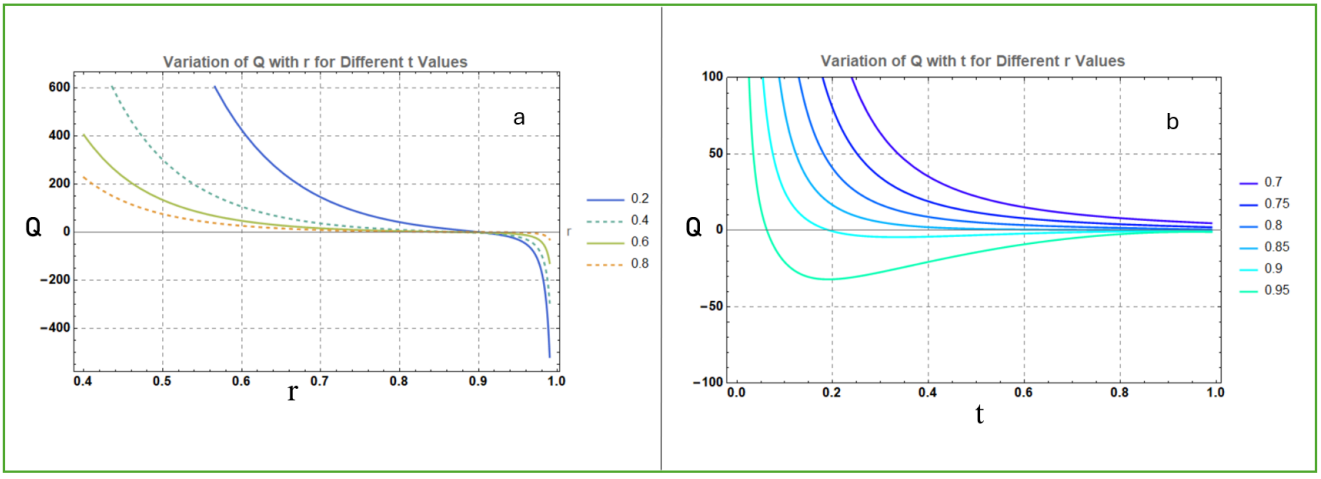


Fig. 2. (color online) Variation of Mendel's Q parameter for $|\psi\rangle$ (a) with r for t=0.2 to 0.8, and (b) with t for r=0.7 to 0.95.

We illustrate the behavior of Mandel's Q parameter, which measures the photon number statistics of the Hybrid Squeezed State (HSS) in Figure 2. This parameter classifies the state's behavior, where $Q = 0$ indicates

classical Poissonian statistics, $Q > 0$ indicates noisy super-Poissonian statistics, and $Q < 0$ indicates quiet, nonclassical sub-Poissonian statistics. Figure 2 (a) shows the variation of Q with the squeezing parameter r for different transmission coefficients t. It reveals that for weak squeezing ($r < 0.9$), the hybrid state exhibits super-Poissonian statistics for all values of t, but for stronger squeezing ($r > 0.9$), the Q value becomes negative, indicating a transition into the nonclassical, sub-Poissonian regime. Figure 2 (b) further explores this by plotting Q against the transmission t for various r values, demonstrating that the largest negative values and thus the most pronounced nonclassical behavior occur for a low transmission range of $0.05 < t < 0.4$. This key finding confirms that the hybrid state is not a simple mixture but can be precisely tuned to be more nonclassical than both of its individual components, the squeezed vacuum state and the photon-added squeezed state.

3.2. Photon- number distribution

The probability of finding 2 n photons in an arbitrary quantum state $|\phi\rangle_1$ is given by the square of the absolute value of the scalar product of the number state $|2n\rangle$ and the superposed state $|\phi\rangle_1$, i.e. [21],

$$P_{2n} := |\langle 2n \mid \phi\rangle|^2 = \frac{|\alpha\langle 2n \mid \xi\rangle + \beta\langle 2n \mid \xi, 2\rangle|^2}{|\alpha|^2 + |\beta|^2 + 2\mathfrak{Re}[\bar{\alpha}\beta\langle \xi \mid \xi, 2\rangle]}, \tag{19}$$

where we have used the following relations to obtain the photon number distribution,

$$\langle 2n \mid \xi\rangle = \left(1 - |\xi|^2\right)^{1/4} \left(\frac{\xi}{2}\right)^n \frac{\sqrt{(2n)!}}{n!} \tag{20}$$

$$\langle 2n \mid \xi, 2\rangle = \frac{\left(1-|\xi|^2\right)^{1/4}}{\sqrt{M_2(|\xi|)}} \left(\frac{\xi}{2}\right)^{n-1} \frac{\sqrt{(2n)!}}{(n-1)!} \tag{21}$$

The photon number distribution, $P(n)$, which plots the probability of finding n photons in the hybrid squeezed state and also serves as key evidence of the system's nonclassical properties is plotted in Figure 3. For classical light, this distribution is a smooth, bell-shaped curve, whereas the presence of strong oscillations—clear dips and peaks in probability—is a definitive signature of nonclassical behavior. Figure 3(a) shows the distribution for different transmission coefficients t, where prominent oscillations are observed specifically for values in the range $0.2 < t < 0.8$. Figure 3(b) illustrates the distribution for varying squeezing parameters r, where significant oscillations appear only at low squeezing, such as $r = 0.2$. This comparative behavior clearly indicates that the photon distribution of the system is more sensitive to changes in the transmission coefficient t than to the squeezing parameter r. The pronounced oscillatory patterns within this mid-range of t values underscore the tunability of the HSS's quantum properties and its enhanced nonclassical character.

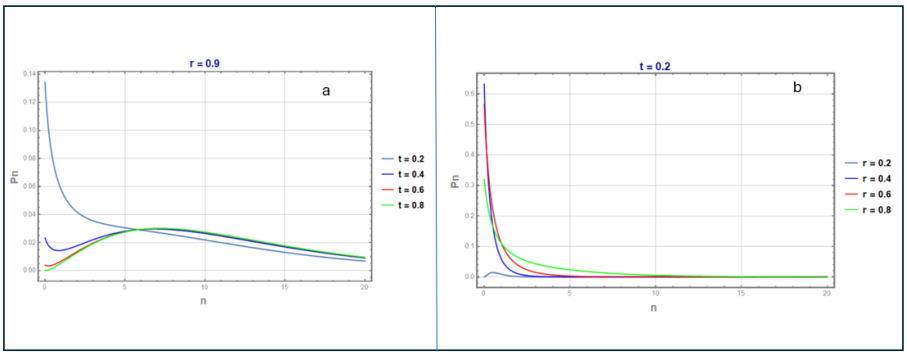


Fig. 3. (color online) Photon number distribution P_n of the hybrid squeezed state (HSS) as a function of photon number n, with fixed Kerr phase shift $\phi_0 = \pi/2$. (a) P_n vs. n for varying transmittance $t = 0.2, 0.4, 0.6, 0.8$ with fixed squeezing parameter $r = 0.9$. (b) P_n vs. n for varying squeezing parameter $r = 0.2, 0.4, 0.6, 0.8$ with fixed transmittance $t = 0.2$. The oscillatory patterns indicate nonclassical behavior.

3.3. Probability distribution function

The probability distribution function (PDF) along the x-quadrature serves as a fundamental tool for characterizing quantum states in continuous-variable quantum systems which is defined as [29]:

$$P(x) = |\langle x|\phi\rangle|^2 \tag{22}$$

Here $|\phi\rangle$ denotes the quantum state vector, $|x\rangle$ represents the eigenstates of the quadrature operator $\hat{x} = (\hat{a} + \hat{a}^\dagger)/\sqrt{2}$ and the squared magnitude yields the probability density for measurement outcomes. For Gaussian states such as coherent and squeezed states, the corresponding PDF takes the standard Gaussian form:

$$P(x) = \frac{1}{\sqrt{2\pi\sigma_x^2}} \exp\left(-\frac{(x - \langle x\rangle)^2}{2\sigma_x^2}\right) \tag{23}$$

The characteristic properties include Symmetric Gaussian curve centred at $x = 0$ with $\sigma_x^2 = 1/2$ for vacuum state and Modified variance $\sigma_x^2 = \frac{1}{2}e^{-2r}$ for Squeezed states. Non-classical states exhibit distinct deviations from Gaussian behaviour includes multiple peaks (e.g., Schroedinger cat states), oscillatory patterns (e.g., photon-added states) and Sub-Poissonian statistics [30]. For a photon-added state created by applying creation operators to a squeezed vacuum state $S(r)|0\rangle$:

$$|r, m\rangle = \mathcal{N}_m \hat{a}^{\dagger m} S(r)|0\rangle \tag{24}$$

where m is the number of added photons and $\mathcal{N}_m$ is the normalization constant. The x-quadrature PDF is:

$$P_m(x) = |\langle x|r, m\rangle|^2 = \mathcal{N}_m^2 x^{2m} |\langle x|S(r)|0\rangle|^2 \tag{25}$$

Now, we want to compute the probability distribution function for HSS Eq. 11, which is obtained as follows:

$$\begin{aligned} P_{(\phi)} &= |\langle x|\phi\rangle|^2 \\ &= \frac{1}{N^2}|\alpha\langle x|\xi\rangle + \beta\langle x|\xi, 2\rangle|^2 \\ &= \frac{1}{N^2}\left|\frac{e^r}{\sqrt{\pi}}\alpha\exp(-x^2e^{2r}) + \frac{4e^{5r}}{3\sqrt{\pi}}x^4\beta\exp(-2x^2e^{2r})\right|^2 \end{aligned} \tag{26}$$

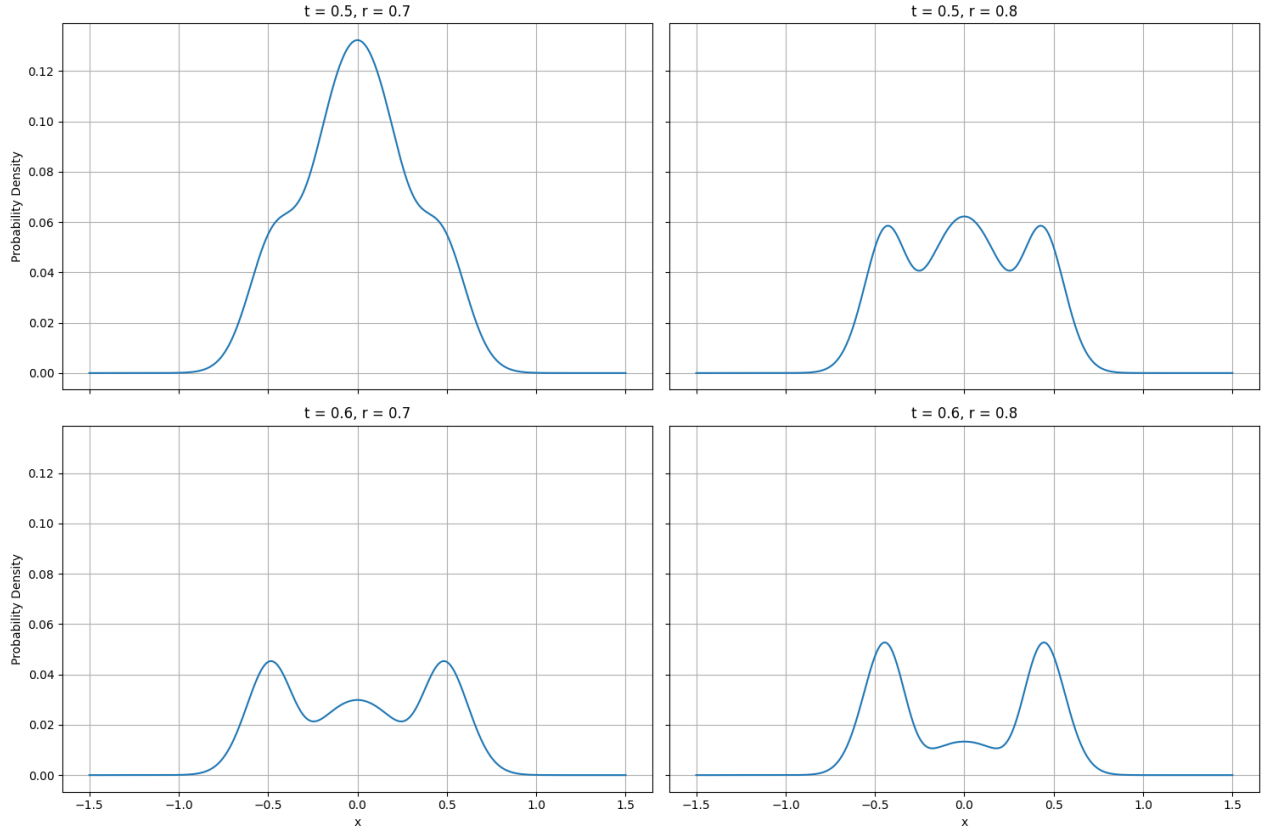


Fig. 4. (color online) PDF for $t = 0.5, 0.6$ and $r = 0.7, 0.8$.

We represent the Probability Distribution Function (PDF) for the electric field's x-quadrature, showing the likelihood of different field measurement outcomes in Figure 4. The figure displays PDFs for different values of the parameters t and r in the hybrid state, with the top row corresponding to $t = 0.5$ for squeezing parameters $r = 0.7$ (left) and $r = 0.8$ (right), and the second row representing $t = 0.6$ for the same r values.

A classical state, like a coherent state, exhibits a PDF that is a simple, symmetric Gaussian bell curve. However, the PDFs for the hybrid state show significant deviations from this Gaussian shape. As the squeezing parameter r increases for a fixed t, the distribution becomes more structured with more pronounced oscillations and multiple peaks–a clear signature of non-classical behavior. Particularly for $r = 0.8$, the appearance of multiple peaks indicates interference patterns in the quadrature distribution. This structured, non-Gaussian shape is a direct visual manifestation of the state's nonclassical character. The results demonstrate that increasing the squeezing strength r actively enhances and shapes the quantum features of the hybrid state, while also highlighting the significant dependency of the photon statistics on both the squeezing parameter r and the transmission parameter t.

3.4. Wigner Function

Another important function is the Wigner function, whose relationship is equal to [31,32].

$$W_{|\phi\rangle}(\eta) = \frac{1}{\pi^2} \int d^2z \ \langle \phi | D(z) | \phi \rangle e^{\bar{z}\eta - z\bar{\eta}} \tag{27}$$

$$= \frac{\int d^2z \left[|\alpha|^2\langle\xi|D(z)|\xi\rangle + |\beta|^2\langle\xi,2|D(z)|\xi,2\rangle + \bar{\alpha}\beta\langle\xi|D(z)|\xi,2\rangle + \alpha\bar{\beta}\langle\xi,2|D(z)|\xi\rangle\right] e^{2(\bar{z}\eta - z\bar{\eta})}}{\pi^2\left(|\alpha|^2 + |\beta|^2 + 2\mathfrak{Re}[\bar{\alpha}\beta\langle\xi \mid \xi,2\rangle]\right)} \tag{28}$$

Wigner quasi-probability distributions presented in Figure 5 provide a comprehensive visualization of the phase-space characteristics of the hybrid squeezed states (HSS) under different squeezing strengths and transmission coefficients. Wigner function $W(\alpha)$ serves as a powerful tool for identifying the presence and degree of nonclassicality, as its negative regions directly signify quantum interference effects that have no classical analog. In this present case, the top row of Figure 5 corresponds to the moderate squeezing regime ($r = 0.4$), while the bottom row depicts the strongly squeezed case ($r = 0.6$). For $r = 0.4$, the squeezed vacuum shows a Gaussian, elliptically deformed distribution without any negativity, reflecting a quasi-classical Gaussian state. However, the two-photon-added squeezed state introduces substantial distortion to this Gaussian profile, leading to the appearance of localized negative regions and oscillatory interference fringes near the phase-space origin. These negative regions arise from higher-order photon-number correlations, which are introduced by photon addition, confirming the transition from a purely Gaussian to a distinctly non-Gaussian state. The hybrid squeezed states at different transmission values ($t = 0.2$ and $t = 0.5$) demonstrate how controlled superposition between these Gaussian and non-Gaussian components modifies the overall Wigner landscape. For smaller transmission ($t = 0.2$), the photon-added component dominates, resulting in the most pronounced negativity ($W_{\min} \approx -0.25$), whereas increasing t enhances the contribution from the squeezed-vacuum component, thereby smoothing the distribution and partially reducing the negative amplitudes. This tunable balance clearly reveals that, for moderate squeezing, there exists an optimal configuration of hybridization that maximizes quantum interference and hence the nonclassical character of such hybrid squeezed states.

In the case of an enhanced squeezing parameter ($r = 0.6$), the overall Wigner landscape becomes significantly more complex, with deep and extended negative regions appearing for all non-vacuum states. The squeezed state with two photos shows stronger negativity and sharper oscillations, whereas the hybrid states display a rich pattern of interference fringes that vary with t. The hybrid configurations at $t = 0.2$, 0.5, and 0.7 reach minimum Wigner values between -0.8 and -1.5, confirming that the depth of negativity scales with the squeezing parameter r. This enhancement results from the amplified quadrature asymmetry and photon-number correlations induced by higher squeezing, which strengthen the interference between the squeezed and photon-added components. The transmission coefficient t primarily governs the spatial distribution and relative intensity of these interference fringes, allowing significant control over the non-Gaussian structure of the state. Thus, the squeezing parameter r determines the maximum attainable nonclassicality, while t acts as a secondary control parameter to control its manifestation in phase space. The strong correlation between r and the depth of Wigner negativity emphasizes the central role of the squeezing parameter in engineering non-Gaussianity of quantum states. In contrast, the modulation by t highlights the flexibility of hybridization for tailoring quantum states. Overall, these results illustrate that hybrid squeezed states constitute a versatile class of engineered non-Gaussian resources, with tunable nonclassical features suitable for continuous-variable quantum information processing, precise measurement of phase estimation, and various applications in quantum sensing that require controlled levels of quantum interference.

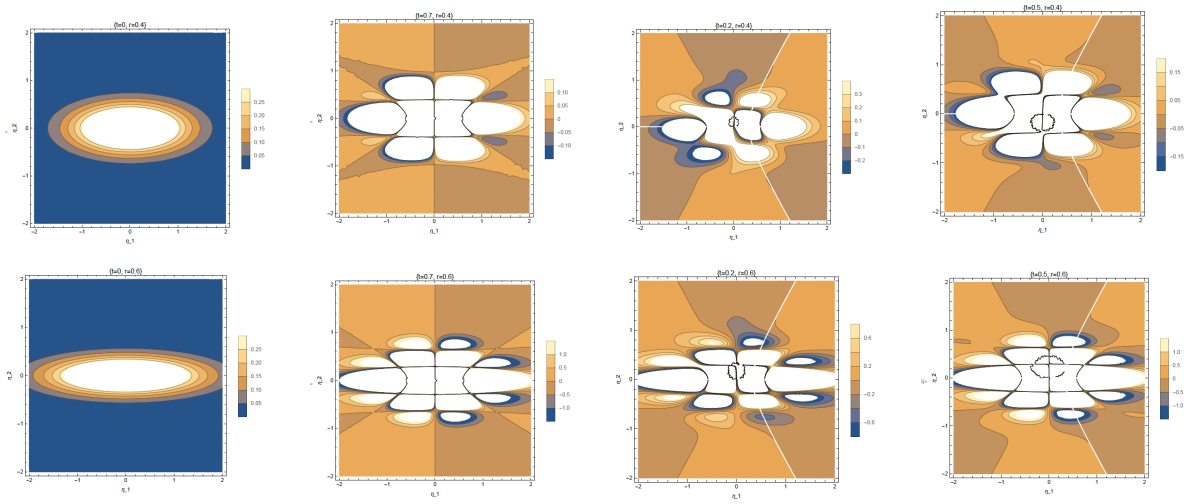


Fig. 5. (color online) Wigner function of different squeezed states: (a) Vacuum Squeezed State ($r = 0.4$), (b) Two-photon added Squeezed State ($r = 0.4$), (c) Hybrid Squeezed State ($t = 0.2, r = 0.4$), (d) Hybrid Squeezed State ($t = 0.5, r = 0.4$), (e) Vacuum Squeezed State ($r = 0.6$), (f) Two-photon added Squeezed State ($r = 0.6$), (g) Hybrid Squeezed State ($t = 0.2, r = 0.6$), and (h) Hybrid Squeezed State ($t = 0.5, r = 0.6$).

4. Phase sensitivity

The strong non-classical character of HSS-evidenced by sub-Poissonian photon statistics, oscillatory photon distributions, and significant Wigner negativity established in Section 3 motivates us to investigate the practical utility of such kind of states for quantum metrology. The connection between these nonclassical indicators and quantum metrology is, however, fundamental, as Wigner negativity is often linked to a state's quantum advantage in Quantum Information Processing. In contrast, the specific form of the photon number distribution directly influences the Quantum Fisher Information. We therefore proceed to evaluate the phase estimation sensitivity of HSS within a Mach-Zehnder interferometer, quantifying how their engineered non-classicality translates into enhanced measurement precision.

Interferometry serves as a fundamental technique for phase shift estimation in optical fields, where the achievable precision is critically dependent on the choice of input quantum states [41]. Whereas classical configurations using coherent states are fundamentally limited by the standard quantum limit (SQL) [33,35], the incorporation of non-classical resources–such as squeezed vacuum states, NOON states, or entangled states in Mach-Zehnder interferometers enables precision measurements that surpass the SQL and approach the ultimate Heisenberg limit. The quantum Cramer-Rao bound (QCRB), obtained from the quantum Fisher information, establishes the theoretical maximum precision for phase estimation and provides the ultimate lower bound on phase sensitivity in a Mach-Zehnder interferometer, i. e. $\delta\theta \geq \delta\theta_{\mathrm{QCRB}}$ [21,37,38]. Recent developments have demonstrated that hybrid input states, which combine hybrid states with coherent light, can further enhance measurement sensitivity beyond classical capabilities.

To investigate this enhancement, we consider a Mach-Zehnder interferometer with input state $|\phi\rangle_{\mathrm{in}} = |\psi\rangle_1 \otimes |\lambda\rangle$, where port 1 receives an hybrid state $|\psi\rangle_1$ and port 2 is fed with a coherent state $|\lambda\rangle = e^{-|\lambda|^2/2} \sum_{k=0}^{\infty} \frac{\lambda^k}{\sqrt{k!}} |k\rangle$ as shown in Figure 6. For such pure input states, the quantum Fisher information that determines the precision of the ultimate phase estimation follows the established formulation [38], providing the foundation for quantifying the metrological advantage offered by hybrid quantum states to surpass the limits of classical measurement.

$$F_{|\Phi\rangle_m}(\theta) = 4\left[\langle\Phi'(\theta)|\Phi'(\theta)\rangle - |\langle\Phi'(\theta)|\Phi(\theta)\rangle|^2\right] \tag{29}$$

Here, $\Phi(\theta)$ and $\Phi'(\theta)$ are defined as:

$$|\Phi(\theta)\rangle = e^{-i\frac{\theta}{2}(a_1^\dagger a_1 - a_2^\dagger a_2)} e^{-i\frac{\pi}{4}(a_1^\dagger a_2 + a_2^\dagger a_1)} |\Phi\rangle_{\text{in}}, \tag{30}$$

$$|\Phi'(\theta)\rangle = \frac{\partial}{\partial\theta}|\Phi(\theta)\rangle = -ie^{-i\frac{\theta}{2}(a_1^\dagger a_1 - a_2^\dagger a_2)} \left(\frac{a_1^\dagger a_1 - a_2^\dagger a_2}{2}\right) e^{-i\frac{\pi}{4}(a_1^\dagger a_2 + a_2^\dagger a_1)} |\Phi\rangle_{\text{in}}. \tag{31}$$

Using the following identity:

$$e^{i\frac{\pi}{4}(a_1^\dagger a_2 + a_2^\dagger a_1)} \left(\frac{a_1^\dagger a_1 - a_2^\dagger a_2}{2}\right) e^{-i\frac{\pi}{4}(a_1^\dagger a_2 + a_2^\dagger a_1)} = -i\left(\frac{a_1^\dagger a_2 - a_2^\dagger a_1}{2}\right) \tag{32}$$

and assuming that the input state at port 2 is a coherent state, such that $a_2|\lambda\rangle = \lambda|\lambda\rangle$, we evaluate the quantum Fisher information function given in equation 10 . Considering the fact that the state $|\psi\rangle_1$ is a linear combination of even kets, we obtain the following result:

$$F_{|\Phi\rangle_{\text{in}}}(\theta) = (2|\lambda|^2 + 1)\langle\psi|a_1^\dagger a_1|\psi\rangle_1 + |\lambda|^2 - \lambda^2\langle\psi|a_1^{\dagger 2}|\psi\rangle_1 - \overline{\lambda}^2\langle\psi|a_1^2|\psi\rangle_1 \tag{33}$$

Thus, the $(\delta\theta_{\text{QCRB}})$ for the mentioned input is given by:

$$\delta\theta_{\text{QCRB}} = \frac{1}{\sqrt{(2|\lambda|^2 + 1)\langle\psi|a_1^\dagger a_1|\psi\rangle_1 - 2\text{Re}[\overline{\lambda}^2\langle\psi|a_1^2|\psi\rangle_1] + |\lambda|^2}} \tag{34}$$

Similarly, the corresponding $\delta\theta_{\text{SQL}}$ and $\delta\theta_{\text{HL}}$ are:

$$\delta\theta_{\text{SQL}} = \frac{1}{\sqrt{{}_1\langle\psi|a_1^\dagger a_1|\psi\rangle_1 + |\lambda|^2}} \tag{35}$$

$$\delta\theta_{\text{HL}} = \frac{1}{{}_1\langle\psi|a_1^\dagger a_1|\psi\rangle_1 + |\lambda|^2} \tag{36}$$

The phase sensitivity diagrams in Figure 7 demonstrate the quantum metrological capabilities of hybrid squeezed states within a Mach-Zehnder interferometer, with performance is being benchmarked against the Standard Quantum Limit (SQL) and the Heisenberg Limit (HL). The Cramer-Rao bound which is relative to the Heisenberg limit and the standard quantum limit, is investigated for four values of the transmission coefficient $t = 0.2, 0.4, 0.6, 0.8$ as a function of changes in the squeezing intensity parameter r. The value $t = 0.2$

corresponds to states near the squeezed vacuum state, while $t = 0.8$ corresponds to states near the two-photon-added squeezed state. Based on the graph in Figure 7, three important conclusions can be drawn. First, as r increases, the sensitivity improves, leading to enhanced performance. Second, at $r = 1$, the Heisenberg limit, the standard quantum limit, and the Cramer-Rao bound approximately become equal. It is noteworthy that for three values of the transmission coefficient, namely $t = 0.2$, 0.4, and 0.8, the quantum Cramer-Rao bound (QCRB) coincides with the Heisenberg limit. However, for $t = 0.6$, the QCRB surpasses the Heisenberg limit, indicating a significant enhancement in phase estimation sensitivity.

This is very well known that quantum Cramer-Rao bound represents the ultimate lower bound on the estimation error achievable with a given quantum state and a specific measurement scheme, as defined by the Fisher information matrix [37,38]. In our calculations, the QCRB is obtained via the quantum Fisher information, which fully accounts for the quantum correlations present in the input states. It is therefore very important to provide a physical interpretation for the observed behavior of the QCRB for $t = 0.6$ in Fig. 7, where the bound falls below the Heisenberg limit (HL). This counterintuitive result originates from the specific quantum structure of the hybrid squeezed states (HSS) under consideration. In this parameter regime, the effective photon number participating in the phase estimation is effectively reduced due to quantum interference effects between the two input ports. As a consequence, the quantum Fisher information increases beyond the value corresponding to the total mean photon number $\langle N \rangle$, leading to a QCRB that satisfies $\delta\theta_{\mathrm{QCRB}} < 1/\langle N \rangle$. This does not violate any fundamental principle, as the Heisenberg limit is not an absolute lower bound for all quantum states, but rather a benchmark for specific classes of states. Such behavior has been previously reported in the literature; for instance, Bohloul et al. [21] observed a similar effect in Fig. 10(b2) for a comparable interferometric setup. Moreover, as earlier discussed in Refs. [21,37,38], the quantum Cramér–Rao bound, derived from the quantum Fisher information, satisfies the general inequality $\delta\theta \geq \delta\theta_{\mathrm{QCRB}}$, and under specific quantum conditions, it can indeed yield values lower than the Heisenberg limit. This confirms that our results are both physically meaningful and consistent with established quantum estimation theory.

The analysis reveals that optimal phase estimation is achieved by the two-photon-added vacuum state without squeezing. This finding may seem counter-intuitive as because squeezing is a cornerstone of quantum metrology however the enhancement originates from a separate mechanism: where squeezing improves sensitivity by redistributing noise between conjugate quadratures, photon addition directly engineers the photon number distribution. For the two-photon-added vacuum state, this creates specific quantum correlations that exhibit exceptional sensitivity to interferometric phase shifts, as reflected in its high Quantum Fisher Information which underscores that the metrologically optimal state depends critically on both the interferometer configuration and input state structure, revealing photon addition as a powerful alternative to squeezing for quantum-enhanced measurements.

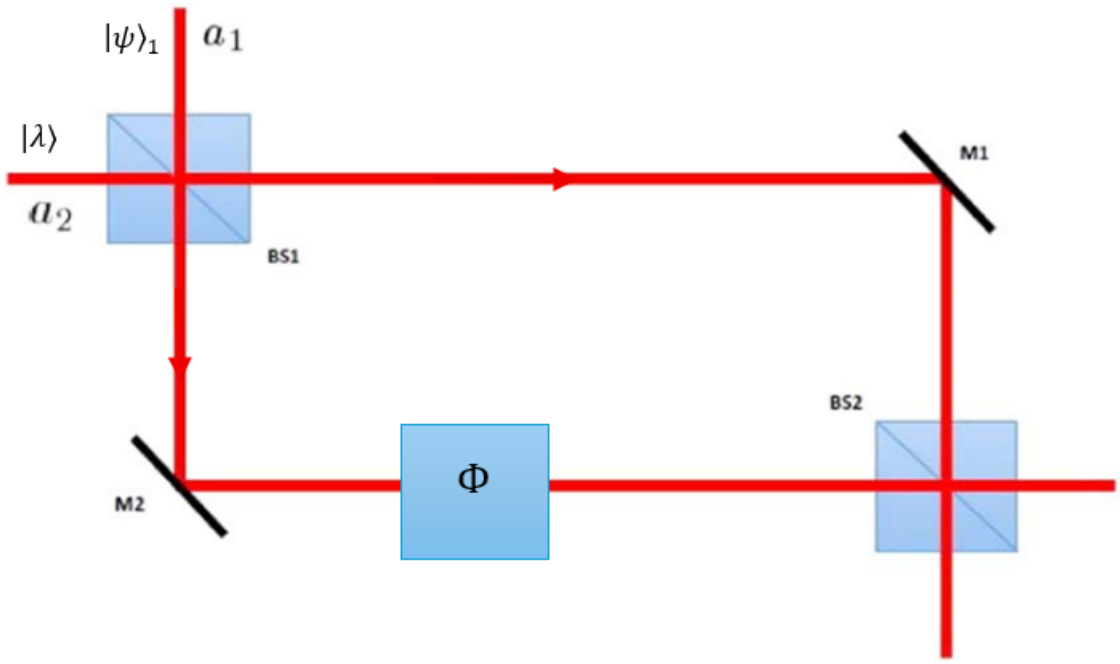


Fig. 6. Schematic for the Mach-Zehnder interferometer. The vertical and horizontal input ports 1 and 2 have been considered for two states $|\psi\rangle_1$ and $|\lambda\rangle$, respectively. The phase element in the upper arm introduces a relative phase θ between the paths and we estimate this phase difference via a suitable observable.

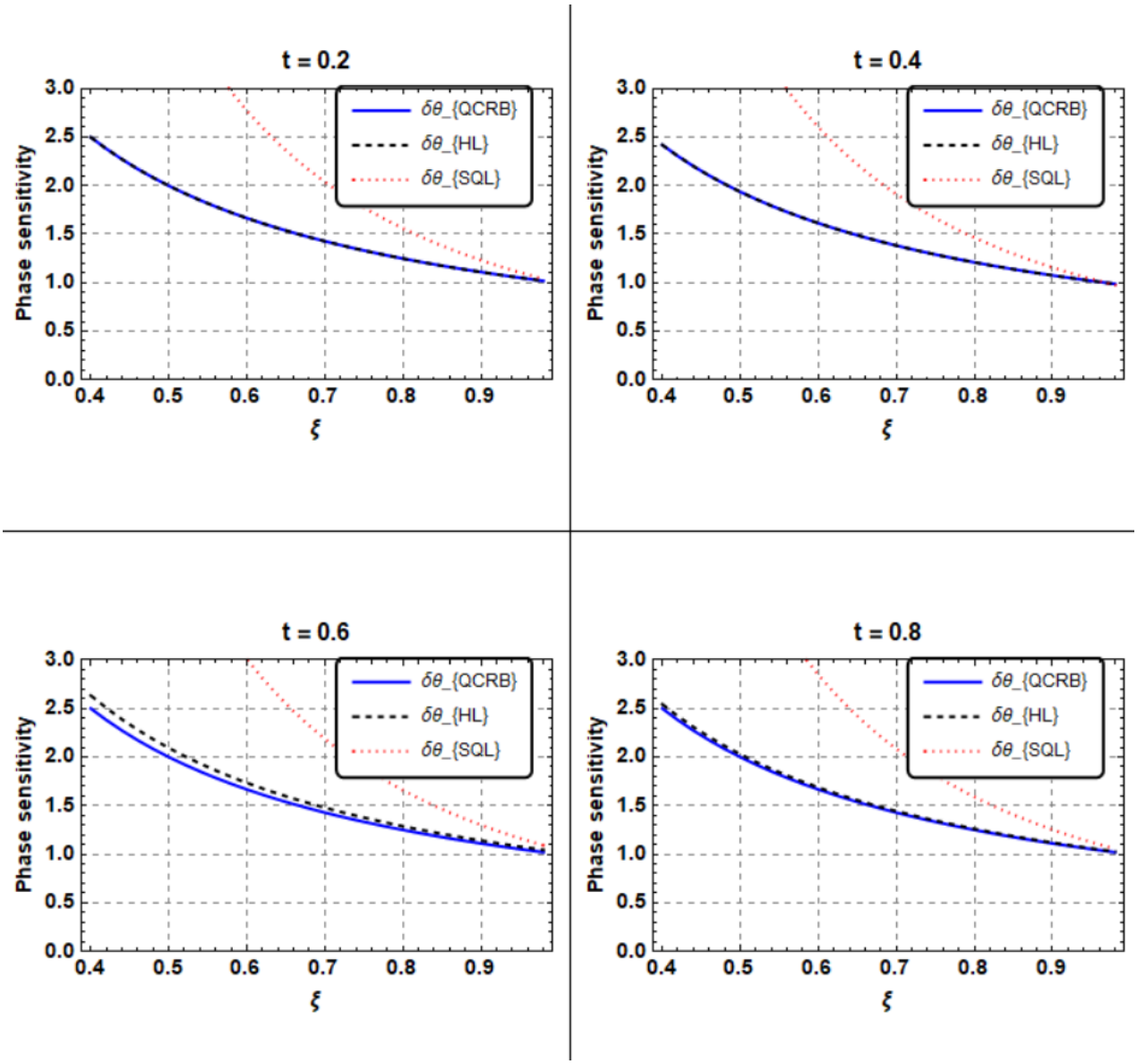


Fig. 7. (Color online) Phase sensitivity plots of the hybrid squeezed state (HSS) in a Mach-Zehnder interferometer, comparing the quantum Cramér–Rao bound (QCRB, solid blue lines), the standard quantum limit (SQL, dotted red lines), and the Heisenberg limit (HL, dashed black lines) as functions of the squeezing parameter r, for four different transmittance values: (a) $t = 0.2$, (b) $t = 0.4$, (c) $t = 0.6$, and (d) $t = 0.8$. All calculations assume a coherent state input at port 2 with amplitude $\lambda = 1$ and optimal Kerr phase shift $\varphi_0 = \pi/2$. In the limit $t \to 0.8$, the state approaches the two-photon-added squeezed state, while in the limit $t \to 0.2$, it approaches the conventional squeezed vacuum state. The QCRB approaches the HL for $t = 0.2$, 0.4, and 0.8 at large r. However, for $t = 0.6$, the QCRB falls below the HL, which arises from the specific quantum structure of the hybrid states, where the effective photon number participating in the phase estimation is reduced due to quantum interference effects. It highlights the rich nonclassical nature of the hybrid states and demonstrates their optimal metrological performance near the two-photon-added squeezed state regime.

5. Experimental Feasibility and Parameter Estimates

The proposed scheme can be implemented using standard quantum optics components that are readily available in current experimental laboratories.

- **Beam splitters (BS1 and BS2):** Commercially available fiber-optic or bulk-optic beam splitters with

tunable splitting ratios can realize the required transmission coefficients in the range $t \in [0, 1/\sqrt{2}]$. Variable beam splitters based on liquid-crystal or piezoelectric actuators provide precise control over the transmission coefficient.

- **Kerr medium:** A nonlinear optical fiber, such as a silica-based photonic crystal fiber, with nonlinear refractive index $n_2 \approx 2.5 \times 10^{-20}\,\mathrm{m}^2/\mathrm{W}$ can provide the required Kerr phase shift $\phi_0 = \chi t$. Experimental measurements have reported the nonlinear refractive index of fused silica in the range $(2.1\text{–}2.7) \times 10^{-20}\,\mathrm{m}^2/\mathrm{W}$ [44], while Kerr nonlinearity at the single-photon level has been experimentally demonstrated in photonic crystal fibers [45].

- **Generation of squeezed states:** Squeezed vacuum states with squeezing parameter r up to 0.8–1.0 (corresponding to approximately 7–9 dB of squeezing) have been experimentally generated using optical parametric oscillators (OPOs) based on periodically poled $KTiOPO_4$ (PPKTP) crystals [46]. In particular, Takeno *et al.* reported -9.01 ± 0.14 dB squeezing at 860 nm using a sub-threshold OPO containing a PPKTP crystal.

- **Phase shifters:** Standard piezoelectric phase shifters and electro-optic modulators can readily provide the required phase shift θ with high precision.

- **Post-selection:** Superconducting nanowire single-photon detectors (SNSPDs) with system detection efficiencies exceeding 95% and dark-count rates below 100 Hz at 1550 nm are commercially available [47]. Their nanosecond dead times and high counting rates make them suitable for implementing the required post-selection measurements in modes b and c. With typical count rates of 10^5–10^6 counts per second, the proposed post-selection procedure can be performed within practical experimental acquisition times.

These realistic parameter estimates demonstrate that the proposed hybrid squeezed-state generation scheme can be implemented using existing quantum optics technology without requiring any fundamentally new experimental components.

6. Conclusion

In this work, we have theoretically investigated the generation, control, and nonclassical properties of hybrid squeezed states (HSS), which combine squeezed vacuum and two photon added squeezed states within a unified framework. We have theoretically demonstrated that through a modified beam splitter-Kerr medium interaction, HSS exhibit strong sub-Poissonian statistics, oscillatory photon number distributions, and pronounced negativity in the Wigner function. All these nonclassical features can be precisely and effectively tuned through the squeezing parameter and the beam splitter transmission coefficients. These results highlight the flexibility and controllability of HSS as nonclassical quantum states. Furthermore, the phase sensitivity analysis within a Mach-Zehnder interferometer revealed that HSS outperform standard squeezed and photon-added squeezed states, enabling precision measurements beyond the standard quantum limit and approaching the Heisenberg limit under optimal conditions. The interplay between tunability, robustness, and enhanced nonclassicality underscores the potential of HSS as a versatile resource for quantum technologies. Unlike the reference scheme [21] , which employs an optical parametric amplifier (OPA) with limited gain-based control, our scheme is based

on a cascaded beamsplitter and Kerr medium arrangement that generates the superposition through a post-selection process. This distinct experimental approach provides two independent control parameters, namely the beam-splitter transmission coefficient (t) and the Kerr phase shift (ϕ_0), enabling precise tuning of the relative weight of the state components from the squeezed vacuum ($t \to 0$) to the two-photon-added squeezed state ($t \to 1/\sqrt{2}$). All components of this scheme, including beam splitters, phase shifters, and Kerr media, are standard and readily available elements in quantum optics laboratories, which makes its experimental implementation simple and practical. In this way, the Kerr medium provides a direct route for controlling the photon-number-dependent phase shift and offers high tunability and versatility compared to previous schemes. Although our study shows that hybrid squeezed states are theoretically superior in ideal circumstances, optical losses and decoherence must be taken into account in real-world applications [39,40,42,43]. Non-classical states with high Wigner negativity, such as the HSS investigated here, are especially susceptible to external interactions, which can quickly destroy their quantum advantage. Future research should carefully study HSS's loss tolerance relative to traditional quantum states, defining the threshold at which their improved performance endures in realistic experimental circumstances. Our study indicates that these hybrid states can play a crucial role in advancing quantum metrology, communication,and enhancing phase sensitivity in optical interferometry up to the Heisenberg limit. Overall, this study establishes hybrid squeezed states as a promising platform for designing next-generation quantum devices with controllable and superior nonclassical properties.

Acknowledgment

Jia-Xin Peng is supported by the National Natural Science Foundation of China (Grant No. 12504566), the Basic Research Program of Jiangsu (Grant No. BK20250947), the Natural Science Foundation of the Jiangsu Higher Education Institutions (Grant No. 25KJB140013), and the Natural Science Foundation of Nantong City (Grant No. JC2024045).

Data Availability Statement

Data sets generated during the current study are available from the corresponding author upon reasonable request.

References

[1] Schnabel, R.: Squeezed states of light and their applications in laser interferometers, Physics Reports**684**,2017

[2] Wodedo, M.A., Tesfahannes, T. G., Darge, T. Y., Pereira, M. and Teklu, B. "Amplifying Two-Mode Squeezing in Nanomechanical Resonators," in IEEE Transactions on Quantum Engineering, vol. 6, pp. 1-15, 2025, Art no. 2100815, doi: 10.1109/TQE.2025.3603459

[3] Zhongzhong Qin, Meihong Wang, Rong Ma, Xiaolong Su. Progress of the Squeezed States of Light and Their Application[J]. Laser and Optoelectronics Progress, 2022, 59(11): 1100001

[4] Abdelmajid El Maaroufi, Manan A, Maroufi B, *et al* 2026 Improving phase sensitivity of SU(1,1) interferometer using even and odd coherent states and squeezed vacuum state, *Physics Letters A* **568**,131231.

[5] Candeloro, A., Razavian, S., Piccolini, M., Teklu, B., Olivares, S., and Paris, M.G.A., 2021. Quantum probes for the characterization of nonlinear media. Entropy, 23, 1353. https://doi.org/10.3390/e23101353

[6] S S Y Chua et al 2014 Class. Quantum Grav. 31 183001

[7] Teklu, B., Ferraro, A., Paternostro, M. et al. Nonlinearity and nonclassicality in a nanomechanical resonator. EPJ Quantum Technol. 2, 16 (2015). https://doi.org/10.1140/epjqt/s40507-015-0029-x

[8] Paris. Matteo, Genoni. Marco, Shammah. Nathan. Teklu, Berihu. (2014). Quantifying the nonlinearity of a quantum oscillator. Physical Review A. 90. 10.1103/PhysRevA.90.012104.

[9] Zelaya, K., Dey, S., Hussin, V., :Generalized squeezed states, Physics Letters A, 382 Issue 47, 2018,

[10] Roy J. Glauber, :The Quantum Theory of Optical Coherence, PhysRev.130.2529,

[11] H. Bergeron, J.-P. Gazeau, P. Siegl, A. Youssef, Semi-classical behavior of P箋schlTeller coherent states. Europhys. Lett. 92, 60003 (2011)

[12] R. Paschotta, article on "Squeezed States of Light" in the RP Photonics Encyclopedia, retrieved 2025-08-26, https://doi.org/10.61835/dcj

[13] U Leonhardt, 2000 Meas. Sci. Technol. 11 1827

[14] Long Ma, Hui Guo, Hengxin Sun, Kui Liu, Bida Su, and Jiangrui Gao, "Generation of squeezed states of light in arbitrary complex amplitude transverse distribution," Photon. Res. 8, 1422-1427 (2020)

[15] Agarwal G S and Tara K Nonclassical properties of states generated by the excitations on a coherent state Phys. Rev. A 43 492-7

[16] Quesne C, Completeness of photon-added squeezed vacuum and one-photon states and of photon-added coherent states on a circle Phys. Lett.A **288** 241-50

[17] Albano L, MundarainDF and Stephany J 2002On the squeezed number states and their phase space representations J. Opt. B: Quantum Semiclass. Opt. 4 **352-7**

[18] Gradshteyn I S and Ryzhik I M 2007 Table of Integrals, Series, and Products (Academic Press).

[19] SelvadorayME 2009 Nonclassicality and photon number distributions in quantum optics IMSc

[20] Shringarpure SUand Franson JD2019 Generating photon-added states without adding a photon Phys. Rev. A 100 043802

[21] M Bohloul et al 2024 Phys. Scr. 99 045112

[22] Y. Turek et al 2023 Phys. Scr. **98** 075103

[23] J. Zhao et al., "Ultra-stable and high-performance squeezed vacuum source enabled via artificial intelligence control," Science Advances, vol. 11, no. 18, p. eadu4888, May 2025, doi: 10.1126/sciadv.adu4888.

[24] L. Gao, L.-a. Zheng, B. Lu, S. Shi, L. Tian, and Y. Zheng, "Generation of squeezed vacuum state in the millihertz frequency band," Light: Science & Applications, vol. 13, p. 294, 2024.

[25] "Bright squeezed light in the kilohertz frequency band," Light: Science & Applications, vol. 14, p. 310, 2025.

[26] Liu, X., Shi, S., Wu, Y. et al. Continuous variable quantum communication with 40 pairs of entangled sideband modes. Sci. China Phys. Mech. Astron. 68, 124211 (2025). https://doi.org/10.1007/s11433-025-2746-x.

[27] L C Kwek and D Kiang 2003 J. Opt. B: Quantum Semiclass. Opt. 5 383DOI 10.1088/1464-4266/5/5/301 Y. Turek et al 2023 Phys. Scr. 98 **075103**

[28] Mandel L, 1979 Sub-Poissonian photon statistics in resonance fluorescence Opt. Lett. 4 **205-7**

[29] SchleichWand Wheeler J A 1987 Oscillations in photon distribution of squeezed states J. Opt. Soc. Am. B 4 **1715-22**

[30] Seyedeh, Robabeh Miry. Mohammad, Javad Faghihi and Hajar, Mahmoudi., 2023 Phys. Scr. 98 125109 DOI 10.1088/1402-4896/ad0813

[31] CahillKE and Glauber R J 1969 Density operators and quasiprobability distributions Phys. Rev. 177 1882-1902

[32] E. P. Wigner (1932). "On the quantum correction for thermodynamic equilibrium". Physical Review. 40 (5): 749-759.

[33] Hariharan P 2003 Optical Interferometry (Elsevier)

[34] Giovannetti V, Lloyd S and Maccone L 2006 Quantum metrology Phys. Rev. Lett. 96 010401

[35] Demkowicz-Dobrzanski R, JarzynaMand Kolodynski J 2015 Quantum limits in optical interferometry Prog. Opt. 60 345-435

[36] Dowling J, AgarwalGS and SchleichWP 1994 Wigner distribution of a general angular-momentum state: Applications to a collection of two-level atoms Phys. Rev. A 49 **4101-9**

[37] Cramer H 1946 Mathematical Methods of Statistics (Princeton University Press)

[38] Rao C R 1945 Information and the accuracy attainable in the estimation of statistical parameters, breakthroughs in statistics: foundations and basic theory Bull. Calcutta Math. Soc. 37 81-91

[39] JarzynaMand Demkowicz-Dobrzanski R 2012. Quantum interferometry with and without an external phase reference Phys. Rev. A 85 011801

[40] M. Frede, R. Wilhelm, D. Kracht, 250 W end-pumped Nd:YAG laser with direct pumping into the upper laser level, Opt. Lett., Vol. 31, No. 6, pp. 3618-3619, **200**

[41] Soorat R., Nitharshini, S., Anil Kumar, M., Singh, S.K., Nonclassical photon statistics and bipartite entanglement generation of excited coherent states. Quantum Inf Process **19**, 297 (2020). https://doi.org/10.1007/s11128-020-02756-9.

[42] Teklu, B., Bina, M., and Paris, M.G.A., 2022. Noisy propagation of Gaussian states in optical media with finite bandwidth. Scientific Reports, 12, 11646. https://doi.org/10.1038/s41598-022-15865-5

[43] Teklu, B., 2022. Continuous-variable entanglement dynamics in Lorentzian environment. Physics Letters A, 432, 128022. https://doi.org/10.1016/j.physleta.2022.128022

[44] D. Vermeulen, *et al.*, "Nonlinear refractive index of fused silica," J. Phys. Photonics **4**, 024001 (2022).

[45] N. Matsuda, H. Le Jeannic, H. Fukuda, T. Tsuchizawa, W. J. Munro, K. Shimizu, and Y. Tokura, "A monolithically integrated polarization entangled photon pair source on a silicon chip," Nature Photonics **3**, 95–98 (2009).

[46] Y. Takeno, M. Yukawa, H. Yonezawa, and A. Furusawa, "Observation of −9 dB quadrature squeezing with improvement of phase stability in homodyne measurement," Optics Express **15**, 4321–4327 (2007).

[47] F. Marsili *et al.*, "Superconducting nanowire single-photon detectors: Physics and applications," Nature Reviews Physics **5**, 287–303 (2023).